Original Article	*Curr. Appl. Sci.*, **2026**, *4*(1): 77-95 DOI: 10.22034/cas.2026.245722	Current Applied Sciences

Study of Gemcitabine Adsorption on the Surfaces of Different Types of Boron Nitride Nanotubes

Mahdiye Poorsargol[1]*, Mansoureh Rakhshanipour[1], Zahra Setayesh-Mehr[2]

[1] *Department of Chemistry, Faculty of Science, University of Zabol, P.O. Box 35856-98613, Zabol, Iran*
[2] *Department of Biology, Faculty of Science, University of Zabol, P.O. Box 35856-98613, Zabol, Iran*
Corresponding author's e-mail: *poorsargol.m@uoz.ac.ir*

Article Information

Received: 05 January 2026
Revised: 09 June 2026
Accepted: 10 June 2026
Published online: 16 June 2026

Keywords

Adsorption
Boron-nitride nanotubes
Gemcitabine
Internal and external surfaces
Molecular dynamics simulations

Abstract

Departing from conventional density functional theory approaches, this study employs, for the first time, molecular dynamics simulations to investigate gemcitabine adsorption on the inner and outer surfaces of BNNTs with five chiralities: (7,7), (8,8), (9,9), (8,6), and (11,0). The primary innovation of this study lies in identifying a "diameter- and chirality-dependent interaction map," which expands upon existing knowledge in three key areas: (i) an "adaptive intra-tubular contact index" showing that at smaller diameters (9.52 Å), Gem interacts via vdW forces from multiple directions inside the nanotube, but primarily through π-π stacking on the exterior; (ii) an inverse relationship between diameter and internal interaction energy (from -250 to -179 kJ/mol as diameter increases to 12.20 Å), termed "multi-directional spatial confinement"; and (iii) the first MD evidence of nanotube structural tilting at diameters below 10 Å to optimize drug binding. The quantitative findings reveal three key innovations: (1) strongest interaction for inner BN (8,6), demonstrating a 2.5-fold greater binding affinity as compared with its outer surface; (2) at 8.61 Å, exhibited the maximum hydrogen bonds (1.011) for narrowest nanotube (11,0) introducing a phenomenon termed "curvature-dependent hydrogen bond density"; and (3) enhanced BN water solubility after drug adsorption, facilitating the development of self-solubilizing nanocarriers. Based on these findings, two practical strategies for drug delivery are proposed: BN (8,6) for strong and stable adsorption, and BN (9,9) with minimal contact area (3.53 nm²) for high drug loading. This work establishes a foundation for future multi-drug simulations and physiological release tracking for smart BNNT-based nanocarriers.

1. Introduction

Gemcitabine (Gem) is a widely utilized antimetabolite and ranks among the most frequently prescribed chemotherapeutic agents globally. As a nucleoside analog, it exhibits potent antiproliferative effects following its

metabolic activation within tumor cells. Once converted to its active triphosphorylated form, Gem disrupts DNA synthesis by incorporating into DNA strands and inhibiting ribonucleotide reductase, an enzyme essential for nucleotide production. These mechanisms effectively inhibit cancer cell proliferation and serve as cornerstones of various oncological treatment regimens. Gem exhibits antitumor activity against certain types of cancer, including metastatic breast, ovarian, testicular, bladder, non-small cell lung (NSCLC), pancreatic cancers, and soft-tissue sarcoma [1, 2]. It can be used as an adjuvant chemotherapeutic in combination with other cytotoxic agents, primarily cisplatin, for some cancers, such as NSCLC. Also, in single-agent form, Gem monotherapy can be used in patients with resectable, locally advanced or metastatic pancreatic cancer. Therefore, this FDA-approved drug has been prescribed as the first-line therapy for pancreatic cancer since 1996 [3, 4]. Nevertheless, the use of combination therapy in the treatment of advanced pancreatic cancer leads to greater survival over Gem monotherapy [5]. Gem is a widely used treatment for pancreatic cancer. Still, its high toxicity, low efficiency, poor membrane permeability, short in-vivo half-life, and severe side effects like anemia or leukopenia have led to research on its nanodelivery approach [6-9].

Nanoscale materials are increasingly being studied for their potential in various biological fields, including drug delivery [10, 11]. Nano-carriers, including nanotubes, have demonstrated significant potential in drug delivery, primarily due to their exceptionally high surface area-to-volume ratio. This unique property enhances drug-loading capacity and facilitates controlled release. Additionally, their nanoscale size allows them to efficiently penetrate cellular membranes, tissues, and even bacterial cells, improving drug targeting and therapeutic efficacy. These characteristics make nanotube-based drug carriers a promising tool for advancing precision medicine and enhancing treatment outcomes across various medical applications [12]. Understanding drug-nanotube interactions is crucial for evaluating drug encapsulation behavior in nanotubes [13]. Drug encapsulation in nanostructures is challenging because it requires drug release near cancer cells without requiring chemical modification [14]. Various nano-carriers have been explored for the targeted delivery of Gem in cancer therapy, with promising results. Nanocarriers such as polymeric, mesoporous silica, solid lipid, micelles, dendrimers, liposomes, magnetic, gold, nano-graphene oxide, carbon nanotubes, and boron nitride nanotubes (BNNTs) have shown promising results for targeted Gem delivery in cancer therapy [15-32].

Nanotubes, such as carbon nanotubes (CNTs) and BNNTs, have gained significant attention in drug delivery research due to their nanoscale dimensions, biocompatible surface properties, and minimal toxicity. Their unique structure enables efficient conjugation with therapeutic molecules, facilitating targeted and controlled drug release. These properties make them promising candidates for enhancing drug stability, bioavailability, and cellular uptake in medical applications [33-36]. Researchers are captivated by the exceptional physicochemical properties of BN nanostructures, which make them ideal drug-delivery carriers [37, 38]. BNNTs are attractive due to their superior thermal conductivity, stability, mechanical strength, oxidation resistance, and electrical insulation. BNNTs, unlike carbon nanotubes (CNTs), have stronger interfacial bonding due to their polarized B-N bonds [37, 39-42]. BNNTs are highly biocompatible and exhibit no significant cytotoxicity, making them safer for biomedical applications. Compared to CNTs, BNNTs offer superior water solubility, which enhances their dispersion in biological environments and improves their potential for drug delivery and other therapeutic uses. The encapsulation of 5-fluorouracil within CNTs and BNNTs has been simulated [43]. It was observed that due to the stronger van der Waals (vdW) interactions between the drug and BN, the drug is adsorbed faster into BN. Also, free-energy calculations indicated greater stability of the encapsulated drug within the BN cavity. The interaction between the

drug doxorubicin and BNNTs is due to vdW attraction [44]. It was observed that nanotubes with diameters greater than 4 nm can serve as efficient drug carriers for targeted doxorubicin delivery in chemotherapy. Zigzag BNNT chirality has a higher solubility than armchair BNNT, making it more suitable for medical applications [45]. BNNTs also exhibit good dispersibility and novel chemical functionality, making them promising candidates for drug delivery in cancer treatment [46]. Molecular dynamics (MD) simulation is a powerful tool for understanding drug delivery processes on a molecular scale [47-54].

MD simulations have been performed to study the encapsulation and release process of Gem from BNNTs (17, 0), (18, 0), and (19, 0) in the presence of gold clusters [32]. The results showed that nanotube size strongly affects the interaction between gold clusters and the nanotube. It was found that vdW interactions play a decisive role in Gem release. Another study showed that Gem can be released from BN by C48B12, and that vdW interactions are the primary driving force in the release process [47]. A density functional theory (DFT) analysis of the adsorption behavior of the anticancer drugs cytarabine and Gem on the surface of BNNTs revealed that these drug molecules exhibit greater stability in a water-based solvent. This finding suggests that BNNTs could serve as effective nanocarriers for drug delivery, enhancing the solubility and bioavailability of these chemotherapeutic agents in biological systems [55]. The analysis of non-covalent interactions showed the role and importance of π-π interactions and hydrogen bonding in the adsorption of drugs on the BN surface. The specific geometry and orientation of the drug molecules influence the stability of drug-loaded BN surfaces. The nature of π-π stacking interactions and hydrogen bonding is crucial in determining the binding strength and overall structural stability. These molecular interactions affect the adsorption efficiency, impacting the effectiveness of BN-based nanocarriers in drug delivery applications [56]. The properties of BNNTs can be significantly enhanced through the adsorption and doping of metal atoms, which makes them ideal candidates for drug delivery applications [57]. Roohi et al. conducted a DFT study to evaluate the effectiveness of aluminum (Al)- and gallium (Ga)-doped BNNTs in sensing and delivering the anticancer drugs cytarabine and Gem. Their research explored how these doped BNNTs influence drug adsorption, stability, and interaction strength, providing insights into their potential as advanced nanocarriers for targeted drug delivery [58]. Both drugs were chemically adsorbed on doped nanotubes, and population analysis showed charge transfer from the drug to the doped nanotubes. The results showed that Al- and Ga-doped BNNTs can be used to sense the drugs cytarabine and Gem. The reaction of pristine BN and Al-doped BN with anticancer drugs cis-platinum and nedaplatin has been studied by DFT [59]. The results showed that these drugs adsorbed well on the Al atom, with significant adsorption energy. Therefore, Al-doped BNNTs are suitable as drug carriers. Akbarzadeh et al. simulated the release of cisplatin from CNTs via penetration by an Ag nanowire [60]. The findings revealed that the vdW interaction between the silver (Ag) nanowire and the BNNT plays a key role in triggering drug release. The release rate was highest at body temperature and in BNNTs with the largest diameters, suggesting that thermal and structural factors influence drug desorption. Additionally, a DFT study on the adsorption of the anticancer drug penicillamine on the outer surface of BNNTs indicated significant charge transfer from the drug molecule to the nanotube. This charge-transfer mechanism could enhance stability and interaction strength, making BNNTs promising candidates for drug-delivery applications [61]. After the adsorption process, the energy gap decreases, thereby increasing the electrical conductivity of the nano-complexes. In the investigation of the energy gap in BNNT and the BN/Gem complex, it has been observed that the energy gap is slightly reduced, thereby slightly increasing the delivery of the nano-drug.

As can be seen, most of the studies conducted in Gem drug delivery have been done using DFT methods. Thus, the present study investigates the interaction between Gem molecules and different BNNTs using MD simulations. Due to the unique structure of BNNTs and the importance of Gem drug, the study investigates the stability of Gem inside and outside BNNTs (7, 7), (8, 8), (9, 9), (8, 6), and (11, 0) with various chiralities. According to the studies, no simulations have been conducted on these structures. Therefore, the findings of this research are innovative. It provides a detailed picture of the interaction, adsorption site, Lennard-Jones (L-J) energies, potential, radial distribution function (RDF) curves, contact surface area, and hydrogen bonding.

2. Materials and Methods

2.1 *Simulation details*

First, the initial structures of BNNTs, including (7, 7), (8, 8), (9, 9), (8, 6), and (11, 0), were generated from the Nanotube Modeler package [62]. The molecular structure of Gem was designed by GaussView 6.0 (Figure 1). The initial structures were optimized at the B3LYP/6-31G(d) level of theory in Gaussian09 [63]. To create the initial configurations of the complexes, Gem molecule was placed in two different positions (i) on the outer surface of BNNTs and (ii) inside BNNTs; the configurations are specified as Gem_{in} and Gem_{out}, respectively. An MD simulation was performed to investigate the dynamic adsorption behavior of Gem on both the external and internal surfaces of BNNTs using the GROMACS 2018.1 software package [64]. In all simulated systems, the BNNT was fixed at the center of the simulation box and restrained from movement by applying a constant force of 1000 kJ/(mol·nm²). The simulation box was then solvated using the SPC/E solvation model to mimic a realistic biological environment. The detailed parameters and specifications of the simulated systems are provided in Table 1.

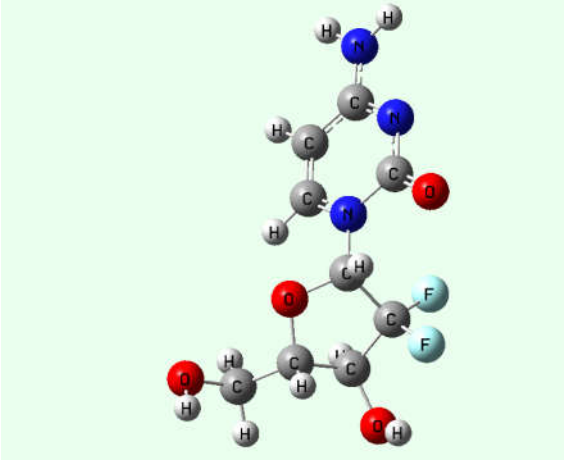

Figure 1. The molecular structure of Gem

The GROMOS 54A7 force field was chosen to model all bonded and non-bonded interactions within the system [65]. The Automated Topology Builder (ATB) was utilized to generate the topology and conformation of Gem [66]. Long-range electrostatic interactions were computed using the particle mesh Ewald (PME) method, while vdW interactions were truncated at a cut-off distance of 1 nm [67].

Before the main MD simulation, the system was carefully prepared with an initial energy minimization using the steepest-descent method. This step was essential to eliminate any steric clashes or unfavorable atomic contacts

that could destabilize the simulation. After minimization, the system underwent a two-phase equilibration. The first phase involved a simulation under canonical (NVT) ensemble conditions, in which the number of particles, volume, and temperature were held constant. This simulation was conducted at 310 K for 200 picoseconds (ps), with temperature control via the Nose–Hoover thermostat to maintain a stable thermal environment. Following the NVT equilibration, the system was further equilibrated under isothermal-isobaric (NPT) conditions for another 200 ps at the same temperature but with pressure maintained at 1 bar using the Parrinello–Rahman barostat. This dual-stage equilibration enabled the system to reach a thermodynamically stable state with respect to temperature and pressure [68,69].

Table 1. Details of the simulated systems

No.	BN (n, m)	BN diameter (Å)	Gem position	No. water	Box dimensions (nm^3)
1	(7,7)	9.49	In	2569	٤ × ٤ × ٥
2	(7,7)	9.49	Out	2569	٤ × ٤ × ٥
3	(8,8)	10.85	In	2558	٤ × ٤ × ٥
4	(8,8)	10.85	Out	2564	٤ × ٤ × ٥
5	(9,9)	12.20	In	3940	٥ × ٥ × ٥
6	(9,9)	12.20	Out	3939	٥ × ٥ × ٥
7	(8,6)	9.52	In	3088	٤ × ٤ × ٦
8	(8,6)	9.52	Out	3077	٤ × ٤ × ٦
9	(11,0)	8.61	In	3127	٤ × ٤ × ٦
10	(11,0)	8.61	Out	3115	٤ × ٤ × ٦

After successful equilibration, the production MD simulation was initiated and run under NPT conditions for 15 nanoseconds (ns). A time step of 1 femtosecond (fs) was used to accurately resolve atomic motions, with the Leap-Frog algorithm employed to integrate the equations of motion due to its efficiency and numerical stability. Periodic boundary conditions were applied in all three spatial directions to mimic an infinite system and eliminate edge effects. Important system properties, including atomic coordinates (trajectories), velocities, and forces, were saved every 10 ps throughout the simulation to enable comprehensive post-simulation analysis. This approach provided a robust framework for analyzing the system's dynamic behavior and structural changes under physiologically relevant temperature and pressure conditions.

3. Results and Discussion

3.1 *Equilibrium state*

The system's equilibrium states were determined using root-mean-square deviation (RMSD) curves, which increased during the first 2 ns and then plateaued over the final 13 ns. The root-mean-square deviation (RMSD) plots in Figure 2 clearly indicate that the simulation time chosen for each system was sufficient to reach equilibrium. The RMSD values stabilized throughout the simulations, indicating that the atomic fluctuations had settled and the systems had reached a steady state. This stabilization confirmed that the structures had adapted to their environments and no longer exhibited significant deviations over time, validating that the systems were appropriately equilibrated before data collection for further analyses.

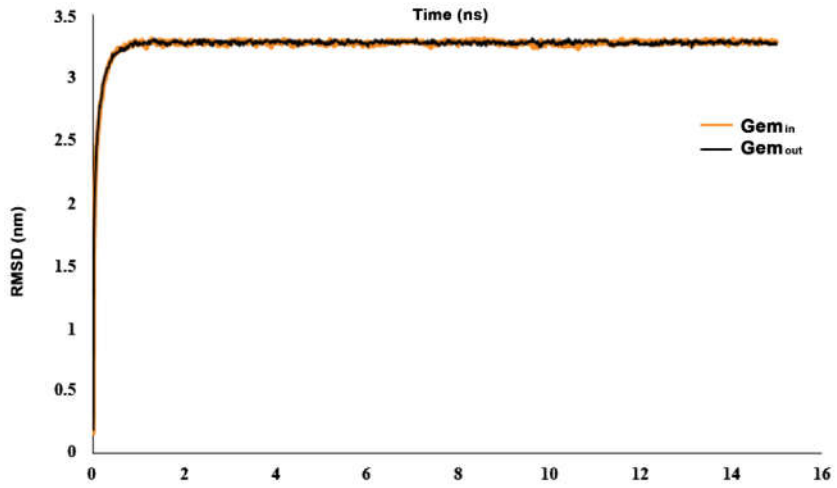

Figure 2. RMSD curves for the two systems with BN (8, 6) as a function of the simulation time

3.2 *Survey of L-J interactions between BN and Gem*

To survey the L-J interactions between BN and Gem, the L-J energy between BN and Gem was obtained (Figure 3). Considering that in both inside and outside positions, all the L-J energy values between Gem and nanotubes are negative, the adsorption of Gem on all nanotubes is thermodynamically favorable proving the existence of attractive interactions between them. As can be seen in Figure 3 (a), the interaction between BN and Gem with the inner surface of BNNTs is stronger than the interaction with the outer surface of BNNTs in all the states, because more B and N atoms are placed around Gem inside BNNTs. By comparing the L-J energy in the inner position of the nanotubes, it can be observed that the highest amount of energy is obtained for the nanotube (8, 6) with a diameter of 9.52 Å. Also, the L-J energy for the nanotubes (7, 7) and (8, 8) has been obtained higher than for the others. Therefore, Gem drug inside these three nanotubes with smaller diameters was found to be more stable. Also, by comparing the L-J energy at the outer position of the nanotubes, it can be seen that the highest energy is obtained for the nanotube (8, 6). This observation is consistent with previous findings indicating that drug adsorption on the external and internal surfaces of BNs is thermodynamically favorable and exothermic [52, 70, 71]. Also, the adsorption of drug molecules was stronger on the inner surface of BNs than on the outer surface of BNs [47, 52, 71].

The number of contacts between BN and Gem over the simulation time is calculated at distances of less than 0.4 nm (Figure 4). As can be seen in Figures 4 (a) and (b), the number of contacts in the case where Gem is placed inside the BN is more than when Gem is placed on the outer surface of the BN. These graphs confirmed that there is a stronger interaction of Gem within the inner surface of BNNTs. Comparison of the number of contacts in the inner position of the nanotubes showed that the number of contacts between Gem and the nanotube increases with the decline in the diameter of the nanotubes. The maximum number of contacts was obtained for the inner position of the nanotube (11, 0). Although the nanotube (11, 0) has the smallest diameter and the highest number of contacts with Gem, it can be seen that its L-J energy with Gem is lower than that of the others. Therefore, Gem is less stable inside this nanotube, probably because of some repulsive interactions between this nanotube and Gem and there appeared to be more contacts for nanotubes (7, 7) and (8, 6). It was also observed that the L-J energy values of (7, 7) and (8, 6) nanotubes with Gem were higher than others, so it can be said that the contacts between these two nanotubes and Gem are attractive.

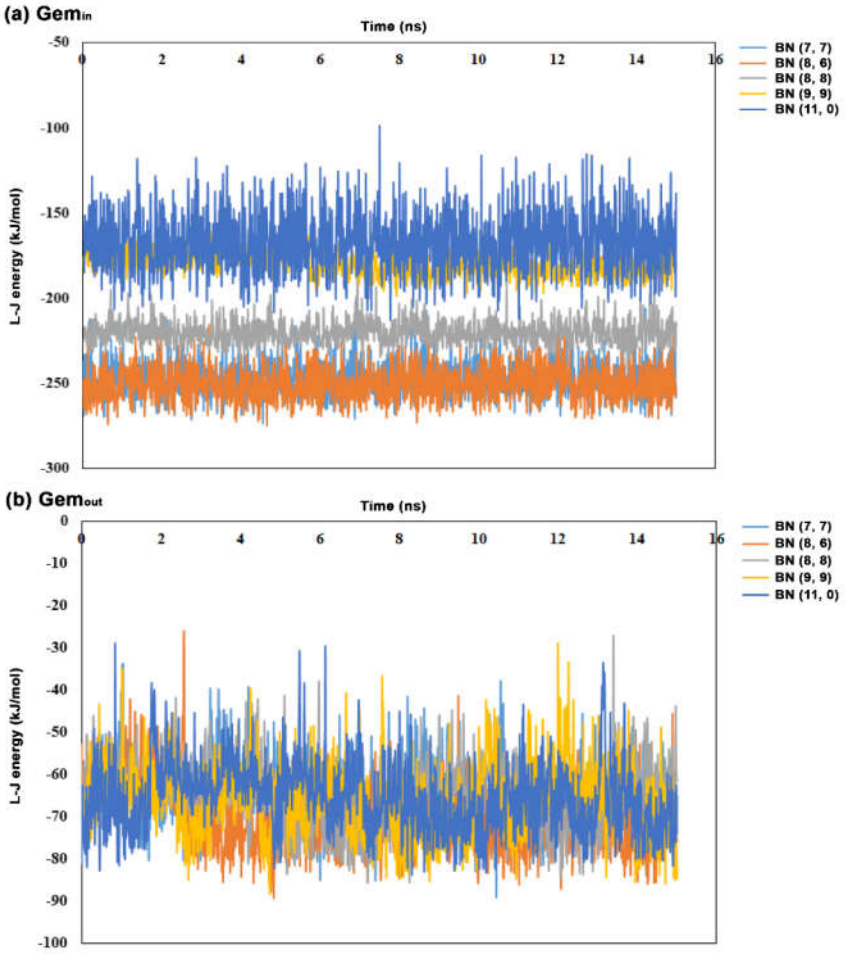

Figure 3. The L-J energy curves between Gem and BN of (a) Gem_{in} and (b) Gem_{out} systems regarding simulation time

The RDF or correlation pair function denoted as g(r) shows the distribution of atoms (molecules) around a particular atom (molecule) and the local structure of the system. As a function of the system temperature and density, g(r) can help determine the probability of identifying a particle within radius r of a reference particle. This function can be derived from the simulations by locating single atoms as a function of time based on MD paths. The RDF graphs of Gem around BN were obtained for all the simulated systems (as in Figure 5). The RDF graphs also show that the value of g(r) for the state where Gem is placed inside BN is higher than g(r) for the state where Gem is placed on the outside surface of BN. So, the possibility of Gem interacting with the inner surface of BN is greater than with the outer surface of BN. Thus, these graphs also confirmed that the interaction between Gem and BN is stronger when Gem is located inside it. Comparison of RDF graphs for the state in which Gem is placed inside BN shows that g(r) for the nanotube (11, 0) has three pronounced peaks located at $r < 0.5$ nm. Therefore, the probability of Gem's presence at this distance inside the nanotube (11, 0) is high. This observation is not far from expected, given the small diameter of this nanotube. With increasing nanotube diameter, peak height decreased, but peak widths extended to greater distances from the nanotubes. So, in the nanotube (9, 9) graph, a shoulder appears at $r = 0.6$ nm. Therefore, the presence of Gem is possible at a distance of 0.6 nm from BN (9, 9). A comparison of RDF graphs for the case where Gem is placed outside BN shows that g(r) for all nanotubes has a high peak at a distance of 0.4 nm, so the possibility of Gem presence at this distance from nanotubes is high.

Also, two shoulders have appeared at a distance of 0.6 to 1 nm, which indicates the possibility of Gem presence in these distances. Therefore, the appearance of these two shoulders means that Gem moves away from the surface of the nanotubes and can indicate the greater freedom of movement of Gem on the outer surface of the nanotube.

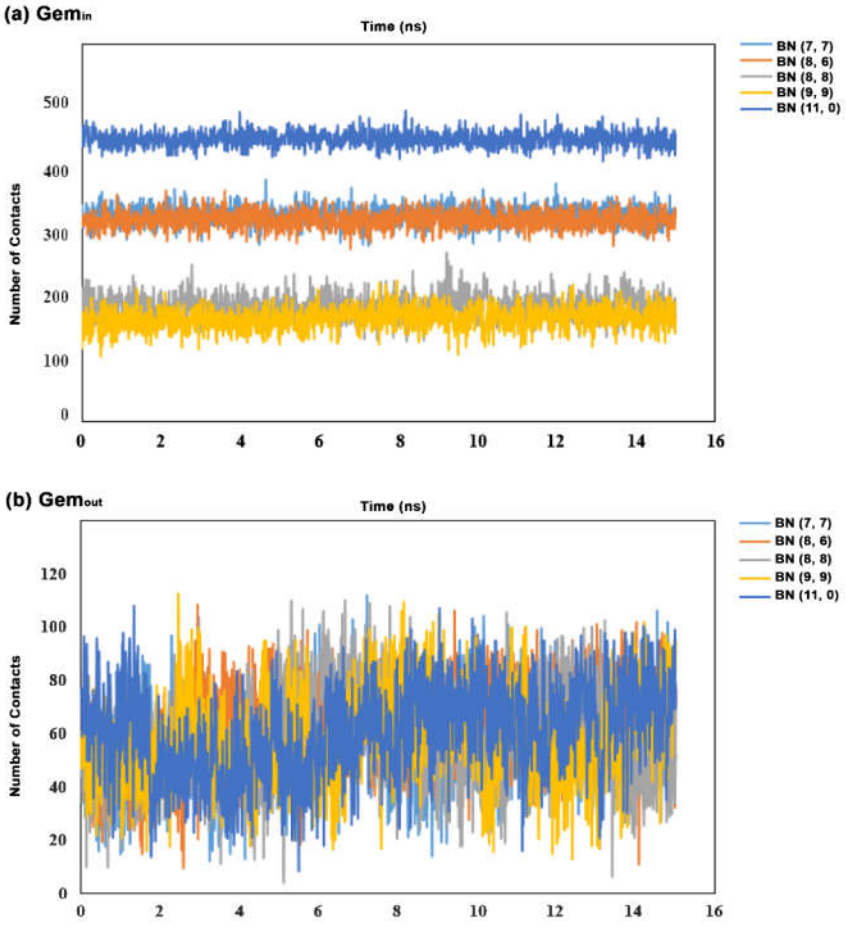

Figure 4. Curve of a number of contact atoms between Gem and BN of (a) Gem_{in} and (b) Gem_{out} systems in terms of simulation time

Figure 3 shows that changes in BN chirality affect the L-J interactions between BN and Gem. The strongest L-J interactions with Gem are related to chiral BN (8, 6). The average L-J energy of BN (8, 6) with Gem is -250 kJ/mol. The weakest L-J interactions with Gem are related to zigzag BN (11, 0). The average L-J energy of BN (11, 0) with Gem is -167 kJ/mol. In the outside position, the strongest L-J interactions with Gem are related to BN (8, 6). In this case, the average energy of L-J is equal to -71 kJ/mol. Therefore, the strength of BN-Gem interactions has changed with the change in BN chirality. It was previously observed that the energy of interactions changes with changes in the chirality of BNs [52]. Changing the diameter of BNs also greatly affects the internal surface interactions. The energy of L-J interactions between Gem and the outer surface of BNs (7, 7), (8, 8), and (9, 9) increased slightly as the diameter increased (the average energy values of these nanotubes are -64, -65, and -66 kJ/mol, respectively). Nonetheless, the energy of L-J interactions between Gem and the inner surface of BNs (7, 7), (8, 8), and (9, 9) decreased as BN diameter increased (the average energy values in this case are -247, -219, and -179 kJ/mol, respectively). The highest interaction energy is associated with the inner surface of BN (7, 7), which is attributed to the suitable curvature of this BN surface for adsorbing Gem. In nanotubes with a smaller

diameter, the number of BN atoms around the drug is larger, and the drug can interact with the nanotube from several directions. By increasing the diameter of the nanotubes, the number of BN atoms around the drug decreases, and the number of favorable interactions between Gem and BN decreases. Ghasempour et al. also showed that the strength of interactions between the nanotube and the drug decreases as the nanotube diameter increases [71].

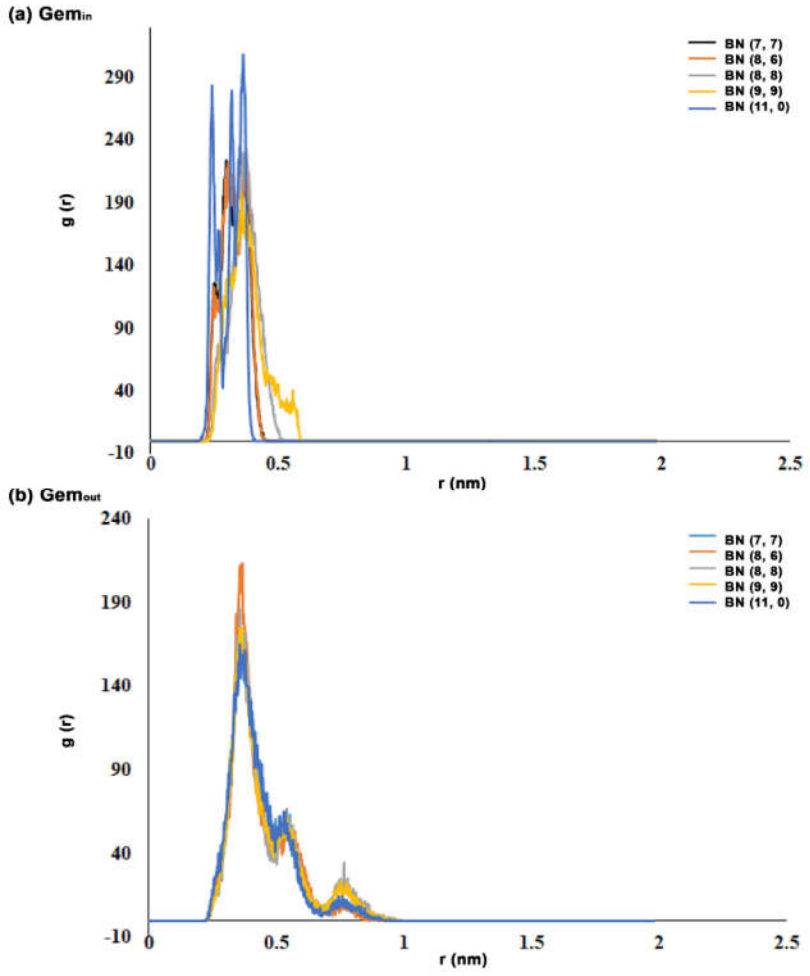

Figure 5. The RDF graphs of Gem relative to BN for (a) Gem_{in} and (b) Gem_{out} simulated systems

The contact surface area for all the simulated systems is computed according to Eq. (1), as presented in Table 2

$$\text{contact surface} = \text{sasa}_{\text{BN}} + \text{sasa}_{\text{Gem}} - \text{sasa}_{\text{comp}} \qquad (1)$$

where $sasa_{BN}$, $sasa_{Gem}$, and $sasa_{comp}$ are the solvent-accessible surface area for BN, Gem, and complex, respectively. As shown in Table 2, the contact surface in the internal position of BN is greater than in its external position. This indicates a higher interaction energy between the nanotube and the drug molecule at the internal position. As can be seen, the highest contact surface areas and interaction energies are associated with the (7, 7) and (8, 6) complexes and the drug molecules. Ghasempour et al. also observed that the contact surface between BN complexes and the drugs paracetamol and phenacetin is higher at the inner position of the nanotube than at the outer position [71]. As the diameter of the boron nitride (BN) nanotube increased, the difference between the contact surfaces at the internal and external positions of the nanotube gradually reduced. This trend aligns with

previous findings, which noted that the interaction energy between the drug molecule and the nanotube at the inner position also decreased with increasing nanotube diameter. As the nanotube diameter decreases, the confined inner space forces the drug molecule closer to the walls, resulting in a greater number of contact points and stronger multidirectional interaction. However, the larger the diameter becomes, the weaker the spatial confinement obtains, allowing the drug molecule to shift from a central position toward the corners or edges of the nanotube. This displacement reduces the proximity and the number of surrounding nanotube atoms available for interaction, leading to a noticeable decline in the overall interaction energy. Table 2 shows that the contact surface of the two BNs (8, 6) and (11, 0) is almost the same because the diameter of these two BNs is almost identical. The energy of their L-J interactions with Gem is still very different due to their different chirality.

Table 2. The contact surface and the average number of hydrogen bonds formed between Gem and BN for all the simulated systems

Position Gem	BN type	Contact surface (nm^2)	Average number of hydrogen bonds
In	(7,7)	4.81	0.099
	(8,8)	4.66	0.060
	(9,9)	3.53	0.036
	(8,6)	4.72	0.078
	(11,0)	4.71	1.011
Out	(7,7)	1.80	0.000
	(8,8)	1.85	0.002
	(9,9)	1.48	0.003
	(8,6)	1.68	0.001
	(11,0)	1.67	0.001

3.3 *Analysis of interactions between different parts of Gem and BN*

Figure 6 shows the final configurations of Gem adsorption on the outer and inner surfaces of BN. As can be seen in the simulation snapshots, BNs (7, 7), (8, 6), and (11, 0) are slightly tilted when Gem was placed inside them. Due to the small diameter of these nanotubes, there is not enough space for Gem; hence, BN changes its structure to achieve favorable interactions with Gem. These structural changes were not observed for BNs with larger diameters (8, 8) and (9, 9). As seen in the snapshots, Gem can interact with the nanotube from all directions on the inner surface of BNs, but on the outer surface, Gem is exposed to water on one side, and its aromatic ring is completely directed to BN on the other side. This observation shows that there is a possibility of π-π stacking interactions between the aromatic ring and the surface of BNs. Previous studies had reported this type of interaction between Gem and BN [32, 47]. Roohi et al. also showed the important role of π-π stacking interactions and hydrogen bonding in Gem adsorption on BNNT surface by analyzing non-covalent interactions [55]. The snapshots show that the drug is close to BN from its pyrimidine ring side. Also, the OH groups in Gem structure are oriented towards the BN surface, and a hydrogen bond could likely form between Gem and the BN surface. Analysis of the hydrogen bonding between Gem and BN showed that a hydrogen bond indeed formed. For comparison, we obtained the average number of hydrogen bonds formed between Gem and BN over the simulation trajectory, as shown in Table 2. As per this table, the average number of hydrogen bonds is more in the inner position than in the outer position of BN; in the inner position, Gem molecule is completely in contact with the atoms of the nanotube, while in the outer position, Gem molecule is in contact with the solvent from one side. Therefore, because the number of Gem contacts with BN atoms in the inner surface is higher, the possibility of

hydrogen bond formation is also higher. By comparing the average number of hydrogen bonds in the inner position of the nanotubes, it can be seen that the probability of hydrogen-bond formation increases as the nanotube diameter decreases. Consequently, the average number of hydrogen bonds for BN (11, 0) with a diameter of 8.61 Å is 1.011. This observation is reasonable because the highest number of contacts was also observed for this nanotube. Therefore, its smaller diameter allows it to form more hydrogen bonds with Gem.

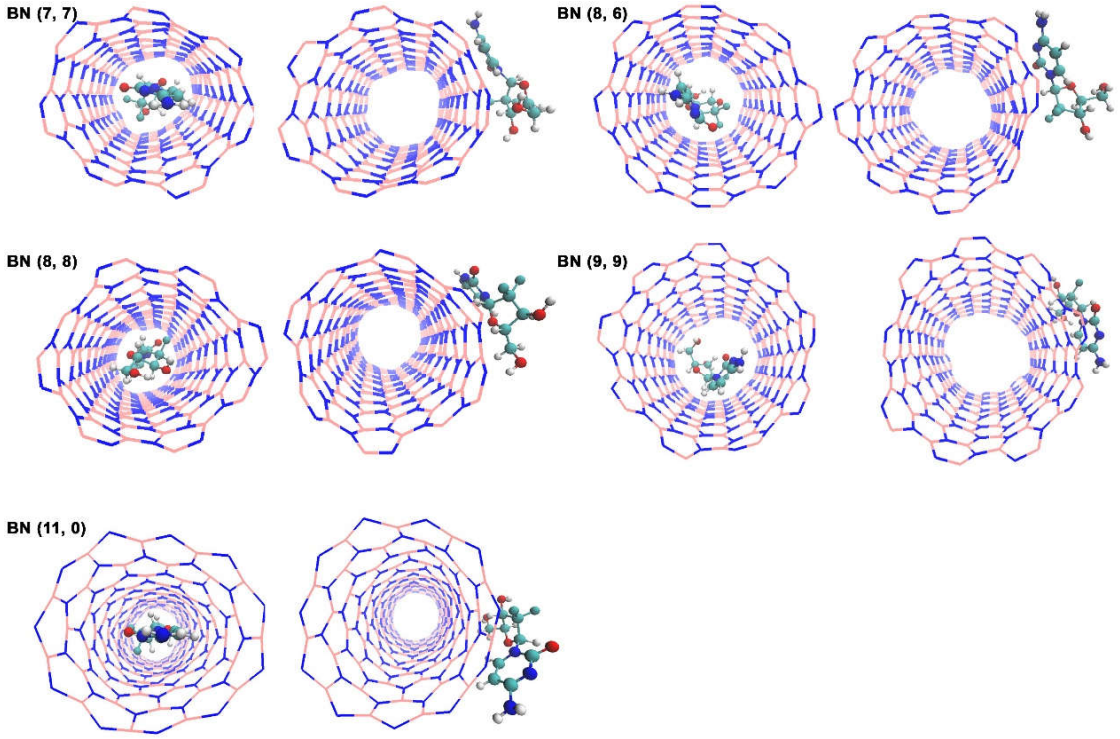

Figure 6. The simulation snapshots of Gem adsorption on the internal and external BNNTs. Water molecules are not shown for clarity

3.4 *Analysis of interaction energy between Gem and system parts in the presence and absence of BN*

The interaction energies (E) between Gem and the system were divided into two types, including free Gem in the solvent and without BN (sys1) and Gem adsorbed on BN in the solvent (sys2), was obtained and presented in Table 3. The interaction energy is the sum of the L-J energy and Coulomb energy between Gem and system parts. In Gem-free system in the solvent: The value of the interaction energy of Gem with itself (Gem-Gem) is -1161.19 kJ/mol, and the value of the interaction energy of Gem with the solvent (Gem-sol) is -337.64 kJ/mol. The sum of these two values in system 1 is equal to -1498.84 kJ/mol. Energy values of Gem bonded to BN in the solvent are collected in Table 3. Comparing the interaction energies of Gem with solvent (Gem-sol) in two systems 1 and 2 shows that in system 2 in the presence of BNs, Gem-sol interaction energy has decreased. This observation confirms that Gem adsorption on the surface of BNs is energetically desirable. The energy difference is equal to Sum E^{sys2} - Sum E^{sys1}. As shown in Table 3, the energy discrepancy between the free and bonded states is greater for complexes in which Gem is adsorbed on the internal surface of BNs. This finding confirms that Gem adsorption on the inner surface of BNs is more efficient than Gem adsorption on the outer surface of BNs in terms of energy.

The maximum discrepancy in these energies is related to BN with a larger diameter and the internal position of BN (9, 9). This observation is in agreement with the above results.

Table 3. The potential energy between Gem and system parts (kJ/mol)

Position Gem	BN type	E (Gem-sol^{sys2})	E (Gem-Gem ^{sys2})	E (BN-Gem ^{sys2})	Sum E^{sys2}	Difference
In	(7,7)	-104.00	-1182.72	-253.93	-1540.66	-41.82
	(8,8)	-161.27	-1183.82	-223.30	-1568.39	-69.55
	(9,9)	-225.61	-1185.03	-181.73	-1592.37	-93.53
	(8,6)	-98.40	-1182.58	-257.45	-1538.43	-39.60
	(11,0)	-189.93	-1175.37	-181.07	-1546.36	-47.53
Out	(7,7)	-310.07	-1163.70	-65.06	-1538.83	-39.99
	(8,8)	-313.39	-1173.28	-65.53	-1552.20	-53.36
	(9,9)	-298.52	-1171.15	-66.36	-1536.02	-37.19
	(8,6)	-305.18	-1161.32	-71.55	-1538.05	-39.21
	(11,0)	-309.02	-1169.39	-66.79	-1545.20	-46.36

E (Gem-Gem ^{sys1}) = -1161.19 kJ/mol; E (Gem-sol^{sys1}) = -337.65 kJ/mol; Sum E^{sys1} = -1498.84 kJ/mol

3.5 *Survey the interaction energy of BN with solvent in the presence and absence of Gem*

The interaction energies between BN and the solvent was obtained in the two states containing free BN in the solvent (BN-sol), without Gem (sys3), and BN bonded with Gem (complex-sol) in the solvent (sys4), as presented in Table 4. The energy difference is equal to E (complex-sol) ^{sys4} - E (BN-sol) ^{sys3}. As can be seen in Table 4, the complex-sol interaction energy in system 4 is higher than the BN-sol interaction energy in system 3. Therefore, it is confirmed that the adsorption of Gem on the surface of BNs enhances the interaction of BNs with water, and this effect is higher when Gem is located at the external position. The energies of complex-sol in the case where Gem is placed on the outer surface of BN are higher than when Gem is placed inside BN. This shows that the adsorption of Gem on BN increased the complex's interactions with water molecules. Therefore, Gem adsorption on the surface of BNs enhances the solubility of BNs in water.

Table 4. The potential energy between the BN and complex (BN-Gem) with solvent (kJ/mol)

Position Gem	BN type	E (BN-sol)^{sys3}	E (complex-sol)^{sys4}	Difference
In	(7,7)	-703.31	-818.66	-115.35
	(8,8)	-832.33	-1005.47	-173.14
	(9,9)	-999.21	-1227.43	-228.22
	(8,6)	-976.28	-1069.54	-93.25
	(11,0)	-1089.16	-1128.91	-39.75
Out	(7,7)	-768.45	-1081.07	-312.62
	(8,8)	-947.88	-1265.48	-317.60
	(9,9)	-1055.95	-1355.44	-299.48
	(8,6)	-1034.01	-1342.09	-308.08
	(11,0)	-1165.87	-1463.42	-297.54

3.6 *Structure-activity relationships (SAR)*

Our findings indicate a nonlinear relationship between the nanotube diameter and the L-J interaction energy at the internal site. As the diameter increases from 9.52 Å (for BNNT (8, 6)) to 12.20 Å (for BNNT (9, 9)), the L-J energy

decreases from -250 to -179 kJ/mol, reflecting a weakening of adsorption attributed to reduced multi-directional contacts and an increased distance between the drug and the nanotube walls. Consistent with previous observations, adsorption of lomustine decreases with increasing diameter of single-walled carbon nanotubes (due to the decrease in contact density) [72]. Nonetheless, for the narrowest nanotube, (11, 0) with a diameter of 8.61 Å, despite having the highest number of contacts (Figure 4) and the highest number of hydrogen bonds (1.011 bonds), the L-J energy is noticeably lower (-167 kJ/mol). This observation suggests that at very small diameters, steric repulsion effects caused by severe spatial confinement overcome vdW attractions. Therefore, an optimal critical diameter appears to exist around 9.5 Å (e.g., BNNT (8, 6)) where the best spatial fit and the highest adsorption energy are achieved. This finding is crucial for designing BNNT-based nanocarriers: very small diameters are unsuitable for encapsulation, while very large diameters also result in poor adsorption. This finding is completely consistent with the results of this paper [73], which emphasizes that for optimal adsorption on BN nanostructures, binding energy and optimal geometry must be considered in conjunction.

Nanotube chirality, as a structural parameter independent of diameter, exerts a significant impact on drug adsorption. Our results show that despite similar diameters for BNNT (8, 6) (9.52 Å) and BNNT (11, 0) (8.61 Å), the L-J interaction energy at the internal site for the chiral type (8, 6) is approximately 50% higher than that of the zigzag type (11, 0) (-250 vs. -167 kJ/mol). This substantial difference can be attributed to the differing spatial arrangement of boron and nitrogen atoms on the nanotube surface. In the chiral (8, 6) configuration, the atomic distribution is such that it facilitates improved structural matching with the pyrimidine rings and functional groups of Gem drug, thereby enabling more effective π-π interactions. In contrast, in the zigzag (11, 0) chirality, despite greater curvature and higher hydrogen bond density, π-π interactions are weaker, and adsorption is primarily driven by hydrogen bonding. Armchair chiralities (7, 7), (8, 8), and (9, 9) also exhibited intermediate behavior. Therefore, the chiral (8, 6) configuration is introduced as the most optimal structure for strong and stable adsorption of gemcitabine.

Our observations revealed that as the diameter decreases --- and consequently, surface curvature increases --- the number of hydrogen bonds formed between Gem and BNNT increases. The highest average number of hydrogen bonds (1.011) was recorded for the narrowest nanotube (11, 0) with a diameter of 8.61 Å. This phenomenon can be attributed to the positioning of the hydroxyl (OH) groups of Gem at a favorable distance and angle relative to the nitrogen atoms (with partial negative charge) and boron atoms (with partial positive charge) on the highly curved surface. The high curvature directs the drug towards the wall and optimizes the spatial orientation of the hydrogen bond donor and acceptor groups. This result is consistent with previous findings regarding an increase in the number of hydrogen bonds with decreasing diameter (and increasing curvature) [74]. This direct relationship between curvature and hydrogen bond density represents a novel finding in the field of BNNT nanocarriers, which can be leveraged to design surfaces with enhanced adsorption capacity for drugs containing hydroxyl groups.

Our results clearly demonstrate that the adsorption site (internal or external) is a primary determinant of interaction stability and nature. In all investigated nanotubes, the L-J energy at the internal site was on average 3 to 4 times greater than that at the external site (e.g., for BNNT (8, 6): -250 vs. -71 kJ/mol). Furthermore, the contact surface area was substantially larger at the internal site (Table 2). This significant difference stems from spatial confinement within the inner cavity: inside the nanotube, Gem is surrounded by BN atoms from all directions and forced into multi-directional contacts, whereas on the external surface, one side of the drug is exposed to the

solvent (water) and interacts only via π-π interactions from one side with the nanotube (Figure 6). From an SAR perspective, this finding suggests two distinct strategies: the internal site is suitable for encapsulation and stable drug carriage (with slow release), while the external surface can be used for applications requiring faster drug release (e.g., local therapies).

Another observation in this study was the deformation of the nanotube itself at critical diameters (below 10 Å). MD simulations showed that BNNTs (7, 7), (8, 6), and (11, 0) undergo significant tilting at the internal site to optimize interactions with Gem (Figure 6). Studies have confirmed the possibility of tilting or deformation of boron nitrides due to interaction with an external molecule [75]. From an SAR perspective for the design of small-diameter nanocarriers, this finding indicates that the structural flexibility of the nanotube should be considered as an influential factor for stability and release behavior.

4. Conclusion

MD simulations were used to investigate the adsorption behavior of the anticancer Gem drug at two different positions on the internal and external surfaces of BNNTs with chiralities (7, 7), (8, 8), (9, 9), (8, 6), and (11, 0). The simulation results showed that Gem is adsorbed in an aqueous medium on both the inner and outer surfaces of BNs due to π-π stacking interactions and hydrogen-bond formation. This adsorption procedure is crucial for drug delivery due to the drug's medical attributes. The results showed that Gem is more strongly adsorbed within BNNTs than outside them, which facilitates encapsulation and drug delivery to target tissues. The results of the present work indicate that BN (8, 6), with a diameter of 9.52 Å and an average energy of -250 kJ/mol, has the strongest interaction with Gem. Therefore, BN (8, 6) can be utilized when a potent interaction is needed between Gem and BNs. In addition, BN (9, 9) with a diameter of 12.20 Å has the lowest contact surface with Gem (3.53 nm^2); therefore, BN (9, 9) can be utilized when a higher drug load is required, and a higher drug load can be obtained from the lower contact surface of BN with Gem and the lowest energy interaction of Gem with the system fragments. In future studies, drug transport and release from these nanotubes can be investigated to gain a better understanding of the possibility of using them as encapsulating agents. Also, because living systems contain multiple drug molecules, it is possible to investigate the adsorption and release of multiple drugs under new conditions.

Acknowledgment

The authors would like to thank University of Zabol for providing financial support for this study (Grant number UOZ-GR-4924).

Conflicts of Interest

The authors declare that there are no conflicts of interest regarding this article.

References

1. Noble S, Goa KL. Gemcitabine: a review of its pharmacology and clinical potential in non-small cell lung cancer and pancreatic cancer. *Drugs* 1997, 54, 447-472.
2. Ciccolini J, Serdjebi C, Peters GJ, Giovannetti E. Pharmacokinetics and pharmacogenetics of Gemcitabine as a mainstay in adult and pediatric oncology: an EORTC-PAMM perspective. *Cancer Chemother. Pharmacol.* 2016, 78(1), 1-12.

3. Burris 3rd HA, Moore MJ, Andersen J, Green MR, Rothenberg ML, Modiano MR, Cripps MC, Portenoy RK, Storniolo AM, Tarassoff P, Nelson R. Improvements in survival and clinical benefit with gemcitabine as first-line therapy for patients with advanced pancreas cancer: a randomized trial. *J. Clin. Oncol.* 1997, 15(6), 2403-2413.
4. Von Hoff DD, Ervin T, Arena FP, Chiorean EG, Infante J, Moore M, Seay T, Tjulandin SA, Ma WW, Saleh MN, Harris M. Increased survival in pancreatic cancer with nab-paclitaxel plus gemcitabine. *N. Engl. J. Med.* 2013, 369(18), 1691-1703.
5. Gresham GK, Wells GA, Gill S, Cameron C, Jonker DJ. Chemotherapy regimens for advanced pancreatic cancer: a systematic review and network meta-analysis. *BMC Cancer* 2014, 14, 1-13.
6. Kurzątkowska K, Santiago T, Hepel M. Plasmonic nanocarrier grid-enhanced Raman sensor for studies of anticancer drug delivery. *Biosens. Bioelectron.* 2017, 91, 780-787.
7. Zhaokai L, Ruobei S, Meichai L, Xinyv W, Xinmei C, Hang C, Xin W, Jianping C. Recent progress in gemcitabine-loaded nanoparticles for pancreatic cancer therapy: a review. *Nanascale* 2025, 17, 17480-17507.
8. Samanta K, Setua S, Kumari S, Jaggi M, Yallapu MM, Chauhan SC. Gemcitabine combination nano therapies for pancreatic cancer. *Pharmaceutics* 2019, 11(11), 574.
9. Dyawanapelly S, Kumar A, Chourasia MK. Lessons learned from gemcitabine: Impact of therapeutic carrier systems and gemcitabine's drug conjugates on cancer therapy. *Crit. Rev. Ther. Drug Carr. Syst.* 2017, 34(1), 63-69.
10. Khan I, Saeed K, Khan I. Nanoparticles: Properties, applications and toxicities. *Arab. J. Chem.* 2019, 12(7), 908-931.
11. Singh P, Chugh V, Banerjee A, Pathak S, Bose S, Nayak R. Nanomaterials: Compatibility towards biological interactions. *In* Practical approach to mammalian cell and organ culture. Singapore: Springer Nature Singapore. 2022, pp. 1059-1089.
12. Din FU, Aman W, Ullah I, Qureshi OS, Mustapha O, Shafique S, Zeb A. Effective use of nanocarriers as drug delivery systems for the treatment of selected tumors. *Int. J. Nanomedicine.* 2017, 12, 7291-7309.
13. Zarghami Dehaghani M, Bagheri B, Yousefi F, Nasiriasayesh A, Mashhadzadeh AH, Zarrintaj P, Rabiee N, Bagherzadeh M, Fierro V, Celzard A. Boron nitride nanotube as an antimicrobial peptide carrier: a theoretical insight. *Int. J. Nanomedicine.* 2021, 16, 1837-1847.
14. Khan MI, Hossain MI, Hossain MK, Rubel MHK, Hossain KM, Mahfuz A, Anik MI. Recent progress in nanostructured smart drug delivery systems for cancer therapy: a review. *ACS Appl. Bio Mater.* 2022, 5(3), 971-1012.
15. Paroha S, Verma J, Dubey RD, Dewangan RP, Molugulu N, Bapat RA, Sahoo PK, Kesharwani P. Recent advances and prospects in gemcitabine drug delivery systems. *Int. J. Pharm.*, 2021, 592, 120043.
16. Singh A, Xu J, Mattheolabakis G, Amiji M. EGFR-targeted gelatin nanoparticles for systemic administration of gemcitabine in an orthotopic pancreatic cancer model, Nanomedicine Nanotechnology. *Biol. Med.*, 2016, 12(3), 589-600.
17. Du C, Qi Y, Zhang Y, Wang Y, Zhao X, Min H, Han X, Lang J, Qin H, Shi Q. Epidermal growth factor receptor-targeting peptide nanoparticles simultaneously deliver gemcitabine and olaparib to treat pancreatic cancer with breast cancer 2 (BRCA2) mutation. *ACS Nano.* 2018, 12(11), 10785-10796.

18. Bhattacharya S, Anjum MM, Patel KK. Gemcitabine cationic polymeric nanoparticles against ovarian cancer: formulation, characterization, and targeted drug delivery. *Drug Deliv.* 2022, 29(1), 1060-1074.
19. Slapak EJ, El Mandili M, Bijlsma MF, Spek CA. Mesoporous silica nanoparticle-based drug delivery systems for the treatment of pancreatic cancer: a systematic literature overview. *Pharmaceutics.* 2022, 14(2), 390.
20. Soni N, Soni N, Pandey H, Maheshwari R, Kesharwani P, Tekade RK. Augmented delivery of gemcitabine in lung cancer cells exploring mannose anchored solid lipid nanoparticles. *J. Colloid Interface Sci.* 2016, 481, 107-116.
21. Al-Mutairi AA, Alkhatib MH. Antitumour effects of a solid lipid nanoparticle loaded with gemcitabine and oxaliplatin on the viability, apoptosis, autophagy, and Hsp90 of ovarian cancer cells. *J. Microencapsul.* 2022, 39(5), 467-480.
22. Wang J, Zhang X, Cen Y, Lin X, Wu Q. Antitumor gemcitabine conjugated micelles from amphiphilic comb-like random copolymers. *Colloids Surf. B Biointerfaces* 2016, 146, 707-715.
23. Qiu Q, Lu D, Liu G, Yang X, Li J, Ren H, Liu J, Sun B, Zhang Y. Colistin Crosslinked Gemcitabine Micelles to Eliminate Tumor Drug Resistance Caused by Intratumoral Microorganisms. *Bioconjug. Chem.* 2022, 33(10), 1944-1952.
24. Öztürk K, Esendağlı G, Gürbüz MU, Tülü M, Çalış S. Effective targeting of gemcitabine to pancreatic cancer through PEG-cored Flt-1 antibody-conjugated dendrimers. *Int. J. Pharm.* 2017, 517(1-2), 157-167.
25. Emamzadeh M, Emamzadeh M, Pasparakis G. Dual controlled delivery of gemcitabine and cisplatin using polymer-modified thermosensitive liposomes for pancreatic cancer. *ACS Appl. Bio Mater.* 2019, 2(3), 1298-1309.
26. Cai W, Geng C, Jiang L, Sun J, Chen B, Zhou Y, Yang B, Lu H. Encapsulation of gemcitabine in RGD-modified nanoliposomes improves breast cancer inhibitory activity. *Pharm. Dev. Technol.* 2020, 25(5), 640-648.
27. Parsian M, Unsoy G, Mutlu P, Yalcin S, Tezcaner A, Gunduz U. Loading of Gemcitabine on chitosan magnetic nanoparticles increases the anti-cancer efficacy of the drug. *Eur. J. Pharmacol.* 2016, 784, 121-128.
28. Devi L, Gupta R, Jain SK, Singh S, Kesharwani P. Synthesis, characterization and in vitro assessment of colloidal gold nanoparticles of Gemcitabine with natural polysaccharides for treatment of breast cancer. *J. Drug Deliv. Sci. Technol.* 2020, 56, 101565.
29. Wei X, Li P, Zhou H, Hu X, Liu D, Wu J, Wang Y. Engineering of gemcitabine coated nano-graphene oxide sheets for efficient near-infrared radiation mediated in vivo lung cancer photothermal therapy. *J. Photochem. Photobiol. B Biol*. 2021, 216, 112125.
30. Eswaran A, Subramanian R, Sivasubramanian G, Gurusamy A. Chitosan Nanoparticle - Montmorillonite - Titanium dioxide Nanocomposites: Synthesis, Characterization, and Antimicrobial Activity. *Iran. Chem. Chem. Eng.* 2023, 42(1), 19-26.
31. Najafi F. Thermodynamic studies of carbon nanotube interaction with Gemcitabine anticancer drug: DFT calculations. *J. Nanostructure Chem.* 2020, 10(3), 227-242.

32. Shafiei F, Hashemianzadeh SM, Bagheri Y. Insight into the encapsulation of gemcitabine into boron-nitride nanotubes and gold cluster triggered release: A molecular dynamics simulation. *J. Mol. Liq.*, 2019, 278, 201-212.
33. Weng Q, Wang B, Wang X, Hanagata N, Li X, Liu D, Wang X, Jiang X, Bando Y, Golberg D. Highly water-soluble, porous, and biocompatible boron nitrides for anticancer drug delivery. *ACS Nano* 2014, 8(6), 6123-6130.
34. Brannon-Peppas L, Blanchette JO. Nanoparticle and targeted systems for cancer therapy. *Adv. Drug Deliv. Rev.* 2004, 56(11), 1649-1659.
35. Ciofani G, Raffa V. Chemically functionalized carbon nanotubes: emerging vectors for cell therapy. *Mini Rev. Med. Chem.* 2009, 9(11), 1251-1261.
36. Ciofani G. Potential applications of boron nitride nanotubes as drug delivery systems. *Expert Opin. Drug Deliv.* 2010, 7(8), 889-893.
37. Kim JH, Pham TV, Hwang JH, Kim CS, Kim MJ. Boron nitride nanotubes: synthesis and applications. *Nano Converg.* 2018, 5, 1-13.
38. Kawaguchi M, Kuroda S, Muramatsu Y. Electronic structure and intercalation chemistry of graphite-like layered material with a composition of BC6N. *J. Phys. Chem. Solids* 2008, 69(5-6), 1171-1178.
39. Kostoglou N, Tampaxis C, Charalambopoulou G, Constantinides G, Ryzhkov V, Doumanidis C, Matovic B, Mitterer C, Rebholz C. Boron nitride nanotubes versus carbon nanotubes: A thermal stability and oxidation behavior study. *Nanomaterials* 2020, 10(12), 2435.
40. Xu T, Zhang K, Cai Q, Wang N, Wu L, He Q, Wang H, Zhang Y, Xie Y, Yao Y. Advances in synthesis and applications of boron nitride nanotubes: A review. *Chem. Eng. J.* 2022, 431, 134118.
41. Turhan EA, Pazarçeviren AE, Evis Z, Tezcaner A. Properties and applications of boron nitride nanotubes. *Nanotechnology* 2022, 33(24), 242001.
42. Baildya N, Mazumdar S, Mridha NK, Chattopadhyay AP, Khan AA, Dutta T, Mandal M, Chowdhury SK, Reza R, Ghosh NN. Comparative study of the efficiency of silicon carbide, boron nitride and carbon nanotube to deliver cancerous drug, azacitidine: A DFT study. *Comput. Biol. Med.* 2023, 154, 106593.
43. Zarghami Dehaghani M, Yousefi F, Mohammad Sajadi S, Tajammal Munir M, Abida O, Habibzadeh S, Hamed Mashhadzadeh A, Rabiee N, Mostafavi E, Saeb M.R. Theoretical Encapsulation of Fluorouracil (5-FU) Anti-Cancer Chemotherapy Drug into Carbon Nanotubes (CNT) and Boron Nitride Nanotubes (BNNT). *Molecules* 2021, 26, 4920.
44. Nejad MA, Umst¨atter P, Urbassek HM. Boron nitride nanotubes as containers for targeted drug delivery of doxorubicin. *J. Mol. Model.* 2020, 26(3), 54.
45. Sánchez SJI, Rivas-Silva JF, García-Toral D. Study of weak interactions of boron nitride nanotubes with anticancer drug by quantum chemical calculations. *Theor. Chem. Acc.* 2020, 139(10), 154.
46. Gao Z, Zhi C, Bando Y, Golberg D, Serizawa T. Noncovalent functionalization of boron nitride nanotubes in aqueous media opens application roads in nanobiomedicine. *Nanobiomedicine* 2014, 1, 7.
47. Roosta S, Nikkhah SJ, Sabzali M, Hashemianzadeh SM. Molecular dynamics simulation study of boron-nitride nanotubes as a drug carrier: From encapsulation to releasing. *RSC Adv.* 2016, 6(11), 9344-9351.

48. Rungnim C, Arsawang U, Rungrotmongkol T, Hannongbua S. Molecular dynamics properties of varying amounts of the anticancer drug gemcitabine inside an open-ended single-walled carbon nanotube. *Chem. Phys. Lett.* 2012, 550, 99-103.
49. Poorsargol M, Poorgalavi M, Samareh HD, Sanchooli M, Karimi P. Molecular Dynamics Simulation of Mixed Surfactants Adsorption on Graphene Nano-Sheets: Effects of Temperature, Electrolyte, and Alcohol. *Iran. Chem. Chem. Eng.* 2022, 41, 4064-4079.
50. Karimi P, Sanchooli M. Investigation of Ability of Graphene Based Nanostructures as Sodium Ion Batteries. *Iran. J. Chem. Chem. Eng.* 2019, 38, 23-30.
51. Karimi P, Poorsargol M, Sanchooli M. Density Functional Theory and Molecular Dynamic Studies About Effects of Functionalization and Surface Modification of Graphene on Adsorption of Phosgene. *Iran. J. Chem. Chem. Eng.* 2023, 42, 2427-2437.
52. Poorsargol M, Setayesh-Mehr Z. Betulinic acid and 3-o-acetyl-betulinic acid interactions with external and internal surface of boron-nitride nanotubes: A DFT and MD investigation. *Comput. Theor. Chem.* 2022, 1213, 113738.
53. Mohammad Alipour F, Babazadeh M, Vessally E, Hosseinian A, Delir Kheirollahi Nezhad P. A Computational Study on the Some Small Graphene-Like Nanostructures as the Anodes in Na–Ion Batteries. *Iran. J. Chem. Chem. Eng.* 2021, 40(3), 691-703.
54. Roosta S, Hashemianzadeh SM, Ketabi S. Encapsulation of cisplatin as an anti-cancer drug into boron-nitride and carbon nanotubes: Molecular simulation and free energy calculation. *Mater. Sci. Eng. C* 2016, 67, 98-103.
55. Roohi H, Facehi A, Ghauri K. Adsorption of cytarabine and gemcitabine anticancer drugs on the BNNT surface: DFT and GD3-DFT approaches. *Adsorption* 2020, 26(8), 1365-1384.
56. Makiabadi B, Zakarianezhad M, Behjatmanesh-Ardakani R, Mousavi SH. Investigating the performance of BN nanotubes as drug delivery systems for Azacitidine and Decitabine anti-cancer drugs: A theoretical study. *Comput. Theor. Chem.* 2024, 1231, 114429.
57. Makiabadi B, Zakarianezhad M, Hosseini SS. Investigation and comparison of pristine/doped BN, AlN, and CN nanotubes as drug delivery systems for Tegafur drug: a theoretical study. *Struct. Chem.* 2021, 32(3), 1019-1037.
58. Roohi H, Rouhi M, Facehi A. Assessing the performance of Al-and Ga-doped BNNTs for sensing and delivering Cytarabine and Gemcitabine anticancer drugs: a M06-2X study. *Mol. Phys.* 2023, 121(22), 1-14.
59. Shakerzadeh E, Noorizadeh S. A first principles study of pristine and Al-doped boron nitride nanotubes interacting with platinum-based anticancer drugs. *Physica E Low Dimens. Syst. Nanostruct.* 2014, 57, 47-55.
60. Akbarzadeh H, Mehrjouei E, Abbaspour M, Salemi S. Ag-Nanowire Diffusion into the Carbon Nanotube: an Efficient Method for Anti-Cancer Drug Release. *Nashrieh Shimi va Mohandesi Shimi Iran* 2017, 36(4), 189-199 (In Persian).
61. Nowroozi A, Shayan K. Investigation of Interaction of Penicillamine Anticancer Drug (Pen) with Armchair Boron Nitride Nanotube. *Nashrieh Shimi va Mohandesi Shimi Iran* 2022, 40(4), 21-32 (In Persian).

62. "Nanotube Modeler (Nanocones, Bucky-Ball, Fullerenes, Simulation Software)." Accessed: Jul. 22, 2024. [Online]. Available: 〈http://www.jcrystal.com/products/wincnt/index.htm.
63. Frisch MJ, Trucks GW, Schlegel HB, Scuseria GE, Robb MA, Cheeseman JR, Scalmani G, Barone VP, Mennucci B, Petersson GA, Nakatsuji H. Gaussian 09, Gaussian. Inc., Wallingford CT. 2009, 121, 150-166.
64. Hess B, Kutzner C, Van Der Spoel D, Lindahl E. GROMACS 4: algorithms for highly efficient, load-balanced, and scalable molecular simulation. *J. Chem. Theory Comput.* 2008, 4(3), 435-447.
65. Schmid N, Eichenberger AP, Choutko A, Riniker S, Winger M, Mark AE, Van Gunsteren WF. Definition and testing of the GROMOS force-field versions 54A7 and 54B7. *Eur. Biophys. J.* 2011, 40(7), 843-856.
66. Stroet M, Caron B, Visscher KM, Geerke DP, Malde AK, Mark AE. Automated topology builder version 3.0: Prediction of solvation free enthalpies in water and hexane. *J. Chem. Theory Comput.* 2018, 14(11), 5834-5845.
67. Darden T, York D, Pedersen L. Particle mesh Ewald: An N log (N) method for Ewald sums in large systems. *J. Chem. Phys.* 1993, 98(12), 10089-10092.
68. Nosé S. A molecular dynamics method for simulations in the canonical ensemble. *Mol. Phys.* 1984, 52, 255-268.
69. Parrinello M, Rahman A. Polymorphic transitions in single crystals: A new molecular dynamics method. *J. Appl. Phys.* 1981, 52(12), 7182-7190.
70. Chermahini AN, Teimouri A, Farrokhpour H. Theoretical studies of urea adsorption on single wall boron-nitride nanotubes. *Appl. Surf. Sci.* 2014, 320, 231-236.
71. Ghasempour H, Dehestani M, Hosseini SM. Theoretical studies of the paracetamol and phenacetin adsorption on single-wall boron-nitride nanotubes: a DFT and MD investigation. *Struct. Chem.* 2020, 31(4), 1403-1417.
72. Cao M, Wu D, Yoosefian M, Sabaei S, Jahani M. Comprehensive study of the encapsulation of Lomustine anticancer drug into single walled carbon nanotubes (SWCNTs): Solvent effects, molecular conformations, electronic properties and intramolecular hydrogen bond strength. *J. Mol. Liq.* 2020, 320, 114285.
73. Shahsavari R, Zhao S. Merger of Energetic Affinity and Optimal Geometry Provides New Class of Boron Nitride Based Sorbents with Unprecedented Hydrogen Storage Capacity. *Small* 2018, 14, 1702863.
74. Mortazavifar A, Raissi H, Akbari A. DFT and MD investigations on the functionalized boron nitride nanotube as an effective drug delivery carrier for Carmustine anticancer drug. *J. Mol. Liq.* 2019, 276, 577-587.
75. Zheng M, Ke C, Bae I, Park C, Smith MW, Jordan K. Radial elasticity of multi-walled boron nitride nanotubes. *Nanotechnology* 2012, 23, 095703.

How to cite this article: Poorsargol M, Rakhshanipour M, Setayesh-Mehr Z. Study of Gemcitabine Adsorption on the Surfaces of Different Types of Boron Nitride Nanotubes. *Curr. Appl. Sci.*, 2026, 4(1):77-95. https://doi.org/10.22034/cas.2026.245722